European Journal of Radiology 120 (2019) 108656

Contents lists available at ScienceDirect

European Journal of Radiology

journal homepage: www.elsevier.com/locate/ejrad

Research article

Amide proton transfer imaging for differentiating benign ovarian cystic lesions: Potential of first time right

Keisuke Ishimatsu[a], Akihiro Nishie[a,*], Yukihisa Takayama[a], Yoshiki Asayama[a], Yasuhiro Ushijima[a], Daisuke Kakihara[a], Koichiro Morita[a], Seiichiro Takao[a], Kenzo Sonoda[b], Yoshihiro Ohishi[c], Hiroshi Honda[a]

[a] Departments of Clinical Radiology, Graduate School of Medical Sciences, Kyushu University, 3-1-1, Maidashi, Higashi-ku, Fukuoka, 812-8582, Japan
[b] Obstetrics and Gynecology, Graduate School of Medical Sciences, Kyushu University, 3-1-1, Maidashi, Higashi-ku, Fukuoka, 812-8582, Japan
[c] Anatomic Pathology, Graduate School of Medical Sciences, Kyushu University, 3-1-1, Maidashi, Higashi-ku, Fukuoka, 812-8582, Japan

ARTICLE INFO

Keywords:
Amide proton transfer imaging
CEST
Ovary
Cyst
ADC

ABSTRACT

Purpose: To investigate whether amide proton transfer (APT) imaging is useful to differentiate benign ovarian cystic lesions.

Materials and methods: This prospective study enrolled a total of 19 lesions in 18 patients with benign ovarian cystic lesion: serous cystadenoma (SCA), n = 4; mucinous cystadenoma (MCA), n = 9; or functional cyst (FC), n = 6. APT imaging was performed with three different presaturation pulse durations: 0.5, 1.0 and 2.0 s. APT signal was defined as magnetization transfer ratio asymmetry at 3.5 ppm. The SI ratios of cyst to muscle calculated on T1- and T2-weighted images were defined as T1- and T2-ratios. Apparent diffusion coefficient (ADC) maps were also generated. We compared the three cystic lesion groups' APT signals, T1-ratio, T2-ratio, and ADC.

Results: When using 2.0 s of presaturation, the APT signals were 1.41 ± 0.71% in SCA, 5.15 ± 1.92% in MCA and 8.52 ± 1.17% in FC. Significant differences were observed between SCA and MCA ($p < .01$) and MCA and FC ($p < .05$), as well as between SCA and FC ($P < .0001$). When 1.0 s presaturation pulse was used, similar results were obtained. On the other hand, ADC value shows significance only between SCA ($2.91 \pm 0.03 \times 10^{-3}$ mm^2/s) and MCA ($2.59 \pm 0.49 \times 10^{-3}$ mm^2/s, $p < .05$). Further, there was no significant difference in the T1-ratio, T2-ratio among the three groups.

Conclusions: APT imaging might be useful for the non-invasive diagnosis of benign ovarian cystic lesions. With the use of the longer presaturation pulse as possible, APT imaging may provide an early and correct diagnosis of ovarian cystic lesions without additional follow-up studies.

1. Introduction

Ovarian cancer is currently one of the most common forms of cancer among women worldwide. In the United States, it is the leading cause of cancer death among gynecologic malignancies, ranking fifth in mortality among all women's cancers (exceeded by breast, colorectum, lung and pancreas) [1]. Some types of benign ovarian cystic lesions such as serous cystadenoma (SCA), mucinous cystadenoma (MCA), endometriotic cyst, and mature cystic teratoma have a malignant potential and can require surgical resection whereas other cystic lesions (e.g., functional cyst) are harmless and require no treatment [2]. It is therefore important to differentiate these benign ovarian cystic lesions as early and correctly as possible to enable an early treatment plan selection and prevent their malignant transformation.

Magnetic resonance (MR) imaging is widely used to evaluate ovarian masses because of its superior tissue contrast [3,4]. Among the benign ovarian cystic lesions, it is easy to diagnose a mature cystic teratoma by using a fat suppression technique, since it basically has a fat component [5]. An endometriotic cyst can also be diagnosed easily since it has a hemorrhagic component and shows high signal intensity (SI) that is not suppressed by fat suppression on a T1-weighted image (T1WI) and typically shows the shading sign in T2-weighted images (T2WI) [6]. In contrast, SCAs, MCAs and Funtional cysts (FCs) can appear as nonspecific cysts and are sometimes difficult to be distinguished because they typically do not have a fat or hemorrhagic component. Thus, although these nonspecific cysts might have

Abbreviations: MR, magnetic resonance; ADC, apparent diffusion coefficient; APT, amide proton transfer; ROC, receiver operating characteristic; SI, signal intensity

* Corresponding author.
E-mail address: anishie@radiol.med.kyushu-u.ac.jp (A. Nishie).

https://doi.org/10.1016/j.ejrad.2019.108656
Received 24 May 2019; Received in revised form 9 August 2019; Accepted 22 August 2019

malignant potential, follow-up by conventional imaging techniques without a therapeutic intervention is often necessary,

Chemical exchange saturation transfer (CEST) imaging has drawn considerable attention as a novel mechanism of MR imaging contrast [7–9]. CEST contrast is achieved by applying a presaturation pulse at the resonance frequency of a slow–intermediate exchanging proton site (−NH, −OH, or metal-bound water molecule) of endogenous or exogenous agents. The resulting saturated or partially saturated spin is transferred to bulk water via chemical exchange. Consequently, specific molecular information is obtained indirectly through the MR imaging signal of tissue water.

Amide proton transfer (APT) imaging is a subset of CEST imaging that refers specifically to the chemical exchange between the protons of free tissue water (bulk water) and amide groups (−NH) of endogenous mobile proteins and peptides [10]. That is, the amount of mobile proteins and peptides can be quantified using APT imaging. The clinical utility of APT imaging for estimating the aggressiveness of solid tumors or treatment effects has been reported [11–17]. We have not been able to identify any study discussing the clinical potential of APT imaging for the evaluation of cystic lesions, but we hypothesized that APT imaging might be useful for the non-invasive histological diagnosis of ovarian cystic lesions since the concentration of mobile proteins/peptides is thought to be different among cystic lesions. Herein, we investigated whether APT imaging is useful to differentiate benign ovarian cystic lesions.

2. Materials and methods

2.1. Patients

This study was approved by our institutional review board and complied with ethical committee standards. Written informed consent was obtained from all patients before their enrollment in the study. From April 2012 to March 2017, a total of 19 lesions in 18 patients (age range, 30–73 years; mean age, 47 years) including SCA (n = 4), MCA (n = 9) and FC (n = 6) were enrolled in the study. All SCA and MCA cases were histologically confirmed after surgical resection. One FC case was also resected with uterine lesion and histologically confirmed. Other FC cases were confirmed by shrinkage on a follow-up scan. The summary flowchart of the patient selection is shown in Fig. 1. The MR examinations were performed within 3 months before surgery for all enrolled patients who underwent surgery. No patients were excluded due to image degradation.

2.2. MR imaging

All MR imaging sessions were conducted in a clinical whole-body 3.0-Tesla MR system equipped with dual-source parallel radiofrequency (RF) transmission technology (Achieva 3.0 T TX; Philips Healthcare, Best, the Netherlands), using a 32-channel torso-cardiac coil. To avoid image degradation due to bowel motion, butylscopolamine (Buscopan 20 mg; Nippon Boehringer Ingelheim, Tokyo, Japan) was injected intramuscularly before imaging. On a single slice delineating the maximum diameter of the lesion, two-dimensional (2D) APT imaging was performed using a presaturation pulse with three different durations: 0.5, 1.0 and 2.0 s (10 × 50, 20 × 50, and 40 × 50 ms, sinc-Gaussian-shaped elements). The saturation power level was fixed to the B_1 root mean square of 2.0 μT. To minimize the B_1 variation during the study, we used a special RF shimming as previously reported [18]. To acquire a z-spectrum, the imaging was repeated at 25 saturation frequency offsets from ω = −6.0 to +6.0 ppm with a step of 0.5 ppm as well as one far-off resonant frequency (ω = −1560 ppm) for signal normalization. The other imaging parameters were as follows: single-shot fast spin-echo readout with driven equilibrium refocusing; repetition time (TR)/echo time (TE), 5000 ms/6 ms; field of view (FOV), 230 × 230 mm; spatial resolution, 1.8 × 1.8 × 5.0 mm^3; slice thickness, 5 mm; echo train length (ETL), 128; sensitivity encoding (SENSE) factor, 2; total scan time, 2 min 20 s for one Z-spectrum. A ΔB_0 map for off-resonance correction was acquired separately using a 2D gradient echo (TR = 14.9 ms, TE = 8.1 and 9.1 ms, flip angle = 30°, number of excitations = 16, scan time = 32 s) with identical spatial resolution, and it was used for pixel-by-pixel ΔB0 correction [19]. The single slice on which the tumor appeared to be the largest was selected as the reference in comparisons to T1WI, T2WI and DWI findings. The details of the other MR sequences are shown in Table 1.

2.3. Data analysis

The z-spectra were fitted through all offsets on a pixel-by-pixel basis followed by the correction for δB inhomogeneity. MTR asymmetry (MTR_{asym}) was defined as:

$$MTR_{asym} = S(-offset)/S - S(+offset)/S,$$

where S(offset) and S are signal intensities (SIs) on the images with a presaturation pulse at 6 to −6 ppm and control (−1560 ppm), respectively. The calculated MTR map at the offset of 3.5 ppm is called the APT-weighted image [9]. APT signals with the presaturation pulse length of 0.5, 1.0 and 2.0 s were defined as APT0.5, APT1.0, and APT2.0, respectively.

$$APT\ signal = S(-3.5ppm)/S - S(+3.5ppm)/S$$

The SI ratios of cyst to muscle (gluteal muscle) calculated on T1WI and T2WI were defined as the T1- and T2-ratios. Apparent diffusion coefficient (ADC) maps were generated referring to the SIs of the DWI with b-values of 0 and 1000s/mm. Regions-of-interest (ROIs) were carefully placed within the cysts adjacent to their edges by two experienced radiologists (A.N. and K.I., with 22 and 8 years of experience in interpreting abdominal MR images, respectively) independently and blinded to the clinical and pathological data. Each radiologist carefully placed as large a polygonal ROI as possible within the cystic mass, avoiding the partial volume effect on the T1WI, T2WI, ADC map, and APT map. The best effort was made to place the ROI at the same region on these images. ADCs were calculated with the commercially available PACS workstation (SYNAPSE; FUJIFILM Medical Co., Ltd., Tokyo, Japan). ROIs were also placed in the gluteal muscle to measure T1- and T2-ratios.

2.4. Statistical analysis

The average values of the APT signals, ADCs, T1-ratio, and T2-ratio measured by the two radiologists were used for the statistical analyses. The interobserver agreement regarding these values was evaluated by the calculation of the intraclass correlation coefficient (ICC). ICCs are considered excellent if greater than 0.74 [20]. The average APT signals, ADCs, and T1- and T2-ratios were compared among the three groups (SCA, MCA, and FC) using Tukey's multiple comparison test (APT0.5, APT1.0 and APT2.0) or Dunn's Kruskal-Wallis multiple comparison test (ADCs, and T1- and T2-ratios) depending on the normality of data. The APT signals with three different presaturation pulse durations in each group were also compared with Dunnett's multiple comparison test. A nonparametric receiver operating characteristic (ROC) analysis was performed to investigate the diagnostic performance of each imaging parameter. All statistical analyses were performed with Prism 5.0 software (GraphPad Software, La Jolla, CA), and p-values < .05 were considered significant.

3. Results

3.1. Patient characteristics

The characteristics of the 19 lesions in 18 patients are summarized in Table 2. There was no significant difference in age among the groups.

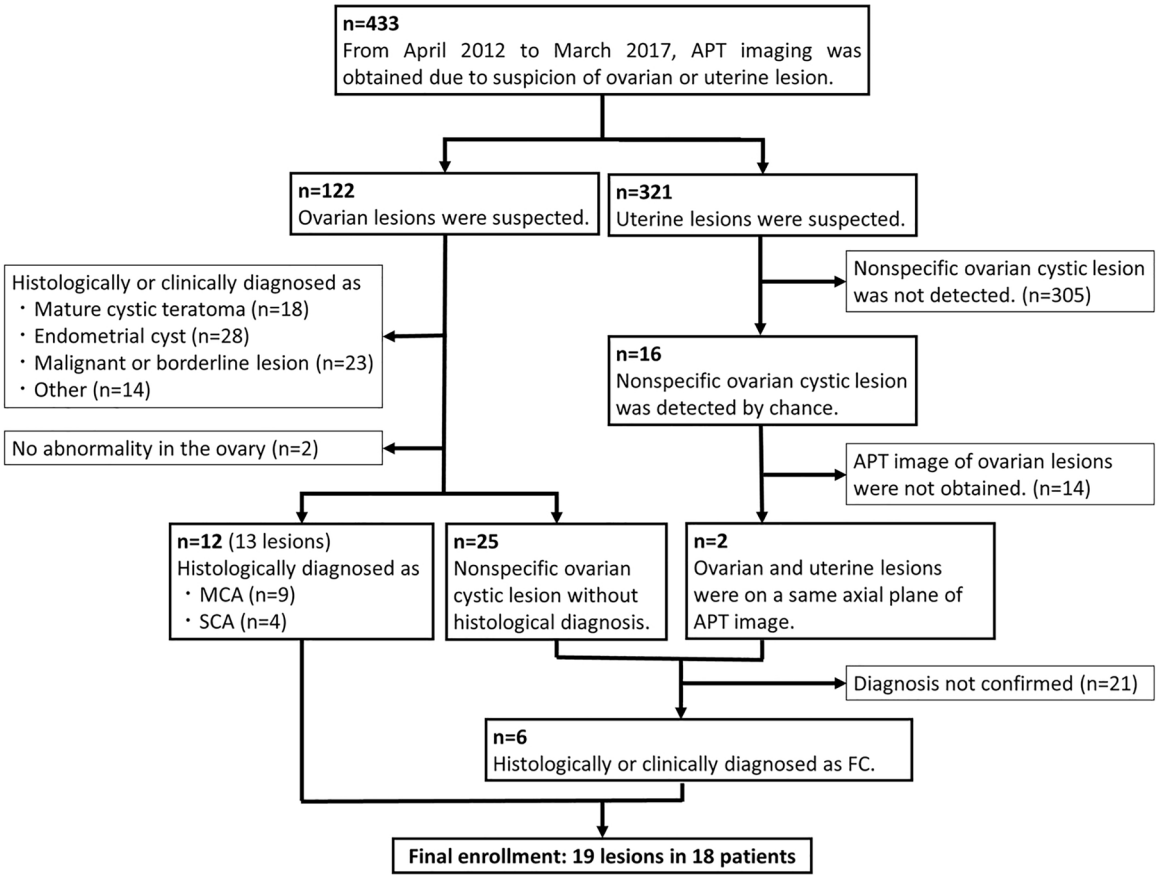

Fig. 1. Patient selection flowchart.

Table 1
Details of other sequence parameters.

Sequence	2D axial T1WI	2D axial T2WI	2D axial DWI
Imaging technique	TSE	TSE	Single shot EPI
Repetition time (ms)	400-650	4000-8000	4000
Echo time (ms)	10	90	55
Flip angle (degree)	90	90	90
Refocus angle (degree)	100	120	N/A
TSE factor	3	17	N/A
EPI factor	N/A	N/A	27
b values (s/mm^2)	N/A	N/A	0, 1000
Field of view (mm)	250 × 250	250 × 250	300 × 300
Spatial resolution (mm^3)	0.625 × 1.0 × 5.0	0.625 × 0.9 × 5.0	3.1 × 4.0 × 5.0
Slice thickness (mm)	5	5	5
Slice gap (mm)	1	1	1
Number of slices	20	20	20
Number of excitations	2	2	2
Fat suppression technique	None	None	SPAIR
Respiratory control	Free breathing	Free breathing	Free breathing
SENSE factor	1	1.3	3
Total scan time (min:sec)	2 min 11 sec	3 min 20 sec	2 min 16 sec

TSE: turbo spin echo, EPI: echo planar imaging, SPAIR: spectral attenuation with inversion recovery.

Table 2
Summary of patient characteristics.

	SCA	MCA	FC
N	4	9	6
Age: median (range)	69 (27-71)	57 (33-72)	38 (31-46)
Longest diameter (mm)	54 ± 6	134 ± 76***	32 ± 12

*** $P < .01$ vs FC by Dunn's Kruskal-Wallis multiple comparison test.

The longest diameter of the MCAs (134 ± 75.8 mm) was significantly larger than that of the FCs (32.3 ± 11 mm, $P < .001$).

3.2. Reproducibility of radiological parameters

The ICCs between the two radiologists were as follows; 0.90 for APT0.5, 0.89 for APT1.0, 0.96 for APT2.0, 0.99 for ADC, 0.98 for T1-ratio, and 0.77 for T2-ratio. The inter-observer agreements were considered excellent in all measurements.

3.3. Presaturation pulse duration and MTR asymmetry

The z-spectra and MTR_{asym} of the SCA (n = 4), MCA (n = 9), and FC (n = 6) groups with three different presaturation pulse durations are shown in Fig. 2. For all three durations, the shape of z-spectrum was steepest in SCA, followed by MCA and FC, which we speculate to indicate a difference in the T2 value in the cyst. The increase in the presaturation pulse duration resulted in decreased SI over the entire range of z-spectra in all of the cystic lesions, which indicated that direct saturation became larger with longer presaturation pulses. The MTR_{asym} values of the MCAs and FCs increased with the duration of the presaturation pulse, whereas that of SCA stayed almost constant.

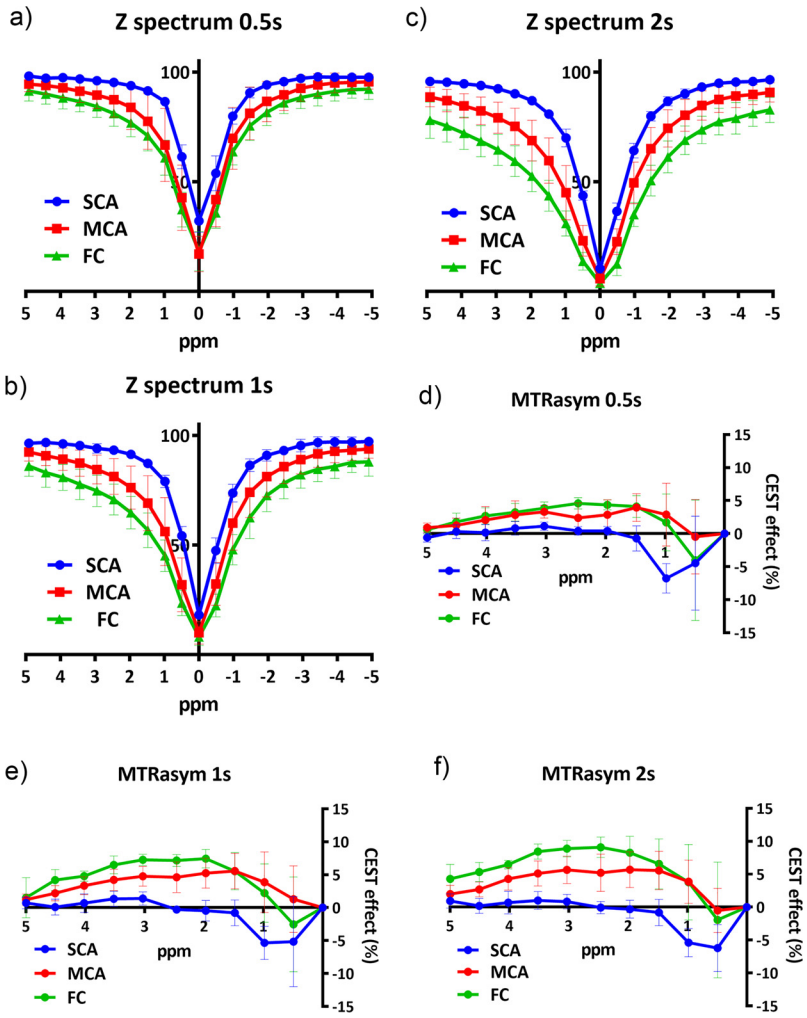

Fig. 2. The z-spectrum (a:0.5 s, b: 1.0 s, c: 2.0 s) and MTR asymmetries (d:0.5 s, e: 1.0 s, f: 2.0 s) in three types of ovarian cystic lesions with three presaturation pulse durations. Mean (SD) are plotted in all figures.

Among the three groups, the SCAs showed the lowest MTR_{asym} over the entire frequency range and with all three presaturation pulse durations. The MTR_{asym} of the MCA group were higher than those of the FC group at smaller frequency offsets (around 1.5 ppm), but the order became the opposite at higher frequency offsets (around 2–4 ppm).

3.4. APT signals, ADCs, and T1 and T2-ratios in the three lesion groups

As the duration of the presaturation pulse became longer, the APT signal significantly increased in the MCAs and FCs whereas it stayed almost constant in the SCAs (Fig. 3). With any length of presaturation pulse duration, the APT signal was highest in the FC group, followed by the MCA and SCA groups. Significant differences in APT1.0 and APT2.0 were observed between the SCAs and MCAs ($P < .05$ in APT1.0 and $P < .01$ in APT2.0) and between the MCAs and FCs ($P < .05$ in APT1.0 and $P < .01$ in APT2.0), as well as between the SCAs and FCs ($P < .001$ in APT1.0 and $P < .0001$ in APT2.0) (Fig. 4a–c). There was no significant difference in the T1-ratio, and T2-ratio among the groups (Fig. 4d–e). The ADC value in SCA was significantly higher than that in MCA ($P < .05$, Fig. 4f). Representative cases are shown in Fig. 5. The averages and standard deviations of the APT signals, T1- and T2-ratios, and ADCs are provided in Table 3.

3.5. ROC analysis

The ROC analysis to distinguish SCAs and MCAs which have malignant potential from FCs which do not have malignant potential showed the areas under the curve in each imaging parameter as follows: 0.65 in APT0.5, (95% CI: 0.39, 0.92), 0.86 in APT1.0, (95% CI: 0.69, 1.03), 0.94 in APT2.0, (95% CI: 0.82, 1.05), 0.66 in T1-ratio, (95% CI: 0.41, 0.91), 0.63 in T2-ratio, (95% CI: 0.38, 0.88), 0.59 in ADC, (95% CI: 0.33, 0.85), respectively. The curves of the ROC analysis are shown in Fig. 6.

4. Discussion

We observed significant differences in APT1.0 and APT2.0 between each pair of the SCAs, MCAs and FCs. ROC analysis showed excellent diagnostic accuracy of APT2.0 for differentiating FCs from SCAs and MCAs. These results might enable us to predict the lesions that have malignant potential from those that require no treatment earlier and more correctly compared to conventional imaging techniques. The APT signal results also showed excellent interobserver agreement between the two radiologists, suggesting high reproducibility. We thus propose that APT imaging can be of clinical use with respect to the reliability of data.

As the duration of the presaturation pulse became longer, a higher APT signal was observed, especially in the MCAs and FCs. CEST imaging is influenced not only by the CEST effect but also by a magnetization transfer (MT) effect and the nuclear Overhauser effect (NOE) [21]. When using longer durations of presaturation pulse, the CEST effect of course increases because the exchanging time is longer.

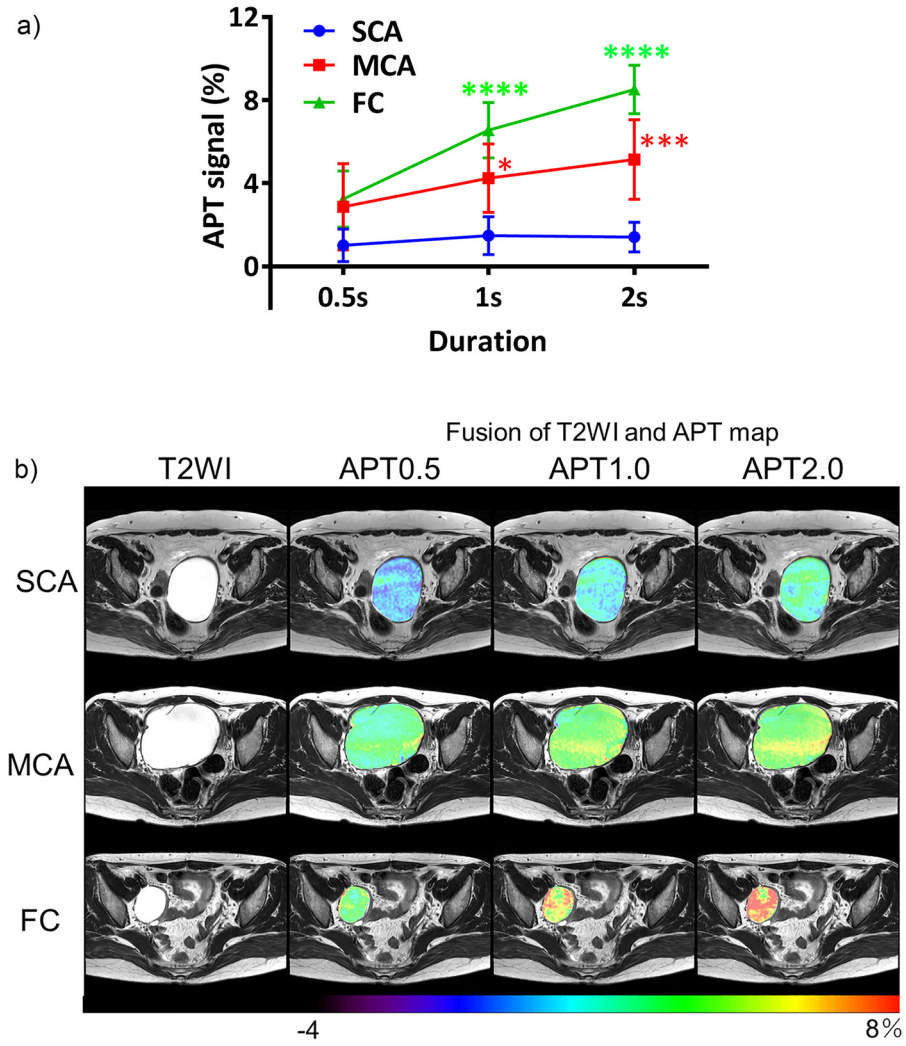

Fig. 3. (a) Relation between the presaturation pulse duration and APT signals in the three types of ovarian cystic lesions. *P < .01, ***P < 0.001, ****P < .0001 vs. 0.5 s by Dunnett's multiple comparison test. Data are presented as mean ± SD. (b) Typical APT0.5, APT,1.0 and APT2.0 maps overlaid on T2WIs of the SCA (*top*), MCA (*middle*), and FC (*bottom*) groups. Color bar indicates APT signal (%).

However, it is known that the CEST signal does not necessarily increase in a solid tumor because the MT effect and/or NOE also increase [19]. By contrast, we speculated that the CEST signal in the present study increased with longer presaturation duration because liquid in the cyst is less influenced by the MT effect or NOE and reflects the CEST effect more directly, unlike solid tumors. Therefore, we believe that a presaturation pulse duration that is as long as possible should be used to obtain a greater CEST signal in cystic lesions, within the restrictions of the specific absorption rate and RF duty cycle.

It is interesting that the APT signal's rate of increase when the duration of presaturation became longer differed among the present three lesion groups. Namely, the FCs were susceptible to the effect of the presaturation duration compared to the MCAs and SCAs. Kikuchi et al. reported that the CEST signal is dependent on the presaturation duration rather than the presaturation power when its proton exchange rate is slow (e.g., amide proton or guanidine proton) [22]. We thus speculate that FCs might have more slow-exchanging protons compared to MCAs and SCAs. Conversely, the liquid in MCAs and SCAs might have more fast-exchanging protons. The concentration of mobile proteins or peptides in SCAs might be too low to show the change of the APT signal even when the presaturation pulse duration is changed.

When the longest presaturation pulse (2.0 s) was used herein, the APT signal was highest in the FCs, followed by the MCAs and SCAs, which showed the most significant difference between each pair of groups. By contrast, the T1-ratio, T2-ratio, and ADC value could not completely distinguish these three types of cystic lesions. The total protein concentration of follicular fluid that is present in FCs was reported to be slightly higher than that of blood [23]. Since Zheng et al. reported that blood showed a very high APT signal (approx. 11%, duration: 1 s, power: 2.8 μT) [24], it would be reasonable that our FC group showed high APT signals (APT2.0: 8.26 ± 1.47%).

There has been no report discussing the concentration of proteins or peptides in MCAs and SCAs, but mucin (which is abundant in MCAs) is a type of glycoprotein that is reported to show a strong CEST signal at 1.0 ppm upfield of the water frequency due to − OH proton and a relatively weak CEST signal around 2–4 ppm upfield of water due to amine proton [25]. We thus speculate that the APT signal in the MCAs examined herein reflected the mucin concentration of fluid in the cysts and demonstrated a certain value. Indeed, the shape of the MTR_{asym} differed between the FCs and MCAs in the present study. Specifically, the peak of the MTR_{asym} in the FCs was around 3.5 ppm whereas the peak in the MCAs was around 1.5 ppm, indicating that the source of the CEST signal might be different between MCAs and FCs as described above. These results suggest that an APT signal at 3.5 ppm may be useful to distinguish MCAs from FCs. We suspect that the concentration of mobile proteins and peptides or another source of the CEST signal are lowest in the SCAs.

A patient's age can be useful to differentiate FC and MCA or SCA

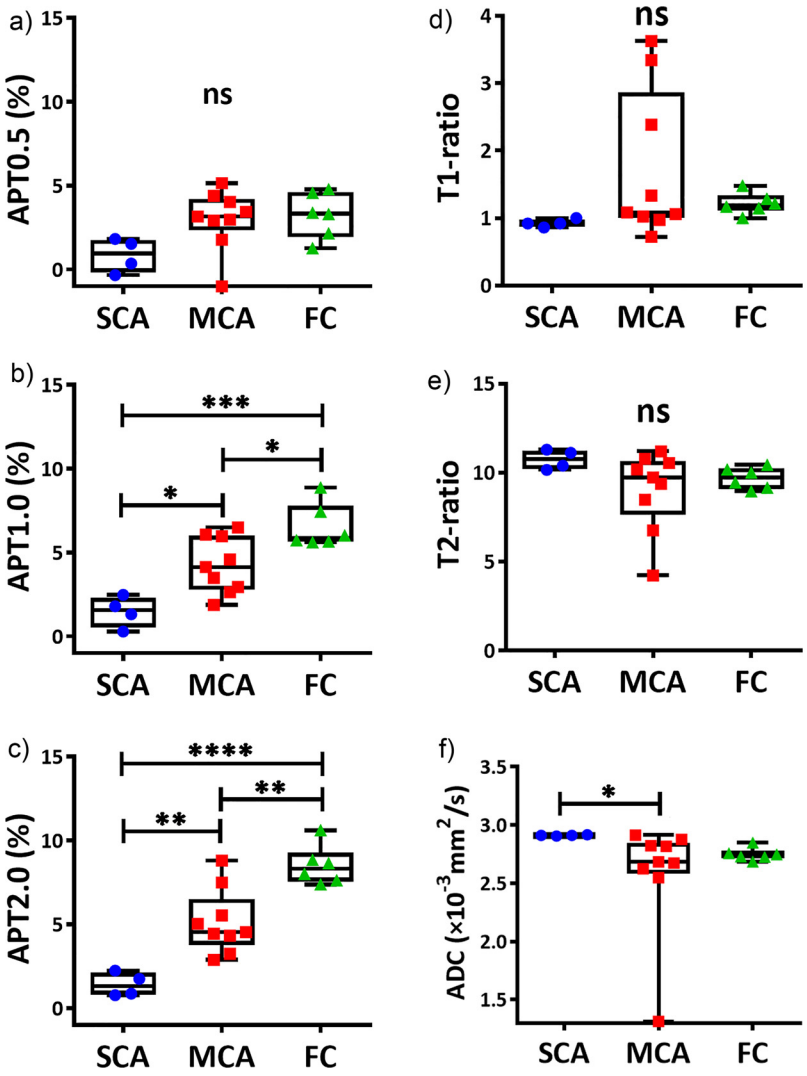

Fig. 4. APT signals with presaturation pulse durations of 0.5 s (a), 1.0 s (b) and 2.0 s (c), the signal intensity ratios of cyst to muscle calculated on T1WI (d) and T2WI (e) and ADC values (f) in the three types of ovarian cystic lesions. Individual points are averages of values calculated by two readers. *P < .05, **P < .01, ***P < 0.001, ****P < .0001 by Tukey's multiple comparison test. Data are presented as mean ± SD.

because FCs usually occur in women of reproductive age whereas SCAs and MCAs can occur in adult women of all ages [4]. However, as there was an overlap between patient groups in the present study, a significant difference in age was not observed although the FC patients tended to be younger than the MCA and SCA patients. The size of cystic lesions can also be used to differentiate FC and MCA or SCA. Indeed, we observed a significant difference in size between the MCAs and FCs, but not between the SCAs and MCAs or the SCAs and FCs, whereas the APT1.0 and APT2.0 showed significant differences between each pair of lesion groups.

Cystic lesions are considered good targets for CEST imaging because the MT effect and NOE are small in the liquid in these lesions. Further, since the T1 values of cystic lesions are longer than those of solid lesions in general, the CEST signal calculated from following equation could be higher.

$$APTsignal = \frac{[amide\ proton]}{[water\ proton]} \cdot T_{1w} \cdot \left(1 - e^{-t_{sat}/T_{1w}}\right) \cdot K \cdot 10^{pH-pKw}$$

We thus believe that APT imaging of a cystic lesion reflects the CEST effect more directly and stronger compared to solid lesions. In addition to benign ovarian cystic lesions, APT imaging can be expected to be applied in the future to ovarian borderline and malignant cystic lesions or cystic lesions in other organs such as retroperitoneal lymphangiomas.

Our study has several limitations. (1) The sample size was small (n = 19). (2) We did not measure the actual protein or peptide concentration or the pH in each cystic lesion. The T1 and T2 values (which could influence the CEST signal) were also not measured, although the T1- and T2-ratios did not show significant differences among the groups. (3) Bowel peristalsis might have caused heterogeneity of the magnetic field and image degradation. However, since we used anticholinergic medication prior to the MR scans, any effect of bowel peristalsis is thought to be limited and no cases were excluded due to image degradation. (4) Only the single slice on which the tumor appeared to be the largest was scanned, due to the limitation of scan time in daily practice. The APT signal calculated by this method may not reflect the characteristics of whole cystic lesion correctly. (5) APT imaging is now being developed and implemented. Although we used a sequence and protocol reported previously [12,13,15,16], these parameters remain to be optimized to obtain more reliable APT signals.

In conclusion, APT imaging might be useful for the non-invasive histological diagnosis of benign ovarian cystic lesions. By using a longer duration of presaturation pulse, amide proton transfer imaging might enable us to predict the ovarian cystic lesions that have malignant potential without follow-up studies.

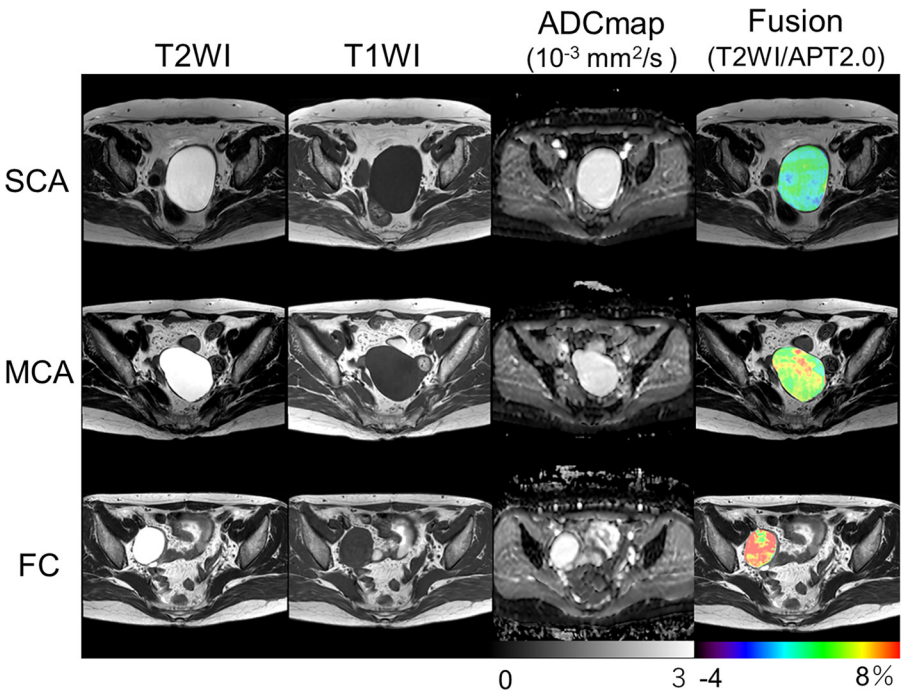

Fig. 5. Typical T2- and T1-weighted images, ADC maps and APT maps (overlaid on T2WI) of an SCA (*top*), MCA (*middle*), and FC (*bottom*). All three cystic lesions showed similar signal intensities in T1WI and T2WI and ADC values. By contrast, the APT signals were clearly different between the types of cyst. The APT values were low in the SCA (2.25%), moderate in the MCA (5.03%) and very high in the FC (7.38%). Color bar indicates APT signal (%).

Table 3
Averages and Standard Deviations of APT signals, T1- and T2-ratios and ADCs.

	SCA	MCA	FC
APT0.5 (%)	0.85 ± 1.01	2.87 ± 2.08	3.24 ± 1.36
APT1.0 (%)	1.48 ± 0.92*,†††	4.25 ± 1.65‡	6.56 ± 1.33
APT2.0 (%)	1.41 ± 0.71**,††††	5.15 ± 1.91‡‡	8.52 ± 1.17
T1-ratio	0.93 ± 0.06	1.72 ± 1.10	1.22 ± 0.16
T2-ratio	10.74 ± 0.55	9.02 ± 2.25	9.69 ± 0.60
ADC ($\times 10^{-3}$ mm^2/s)	2.91 ± 0.03*:	2.59 ± 0.49	2.75 ± 0.05

by Tukey's multiple comparison test (APT0.5, APT1.0 and APT2.0) or Dunn's Kruskal-Wallis multiple comparison test (T1- and T2-ratios and ADCs).

* $P <$ .05.
** $P <$ .01 vs MCA.
††† $P <$ .001.
†††† $P <$ .0001 vs FC.
‡ $P <$ .05, ‡‡: $P <$ .01 vs FC.

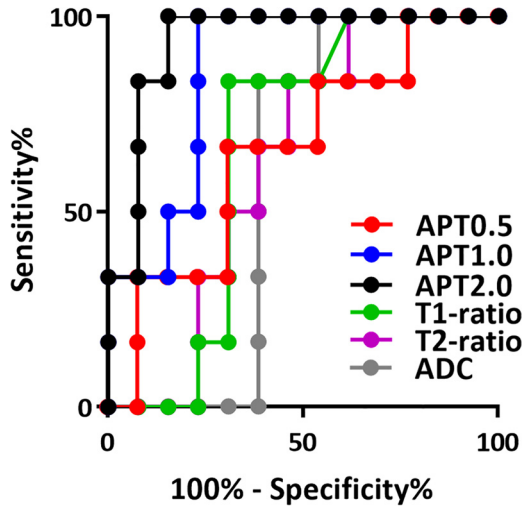

Fig. 6. Curves show APT signals, T1-ratio, T2-ratio and ADCs by using receiver operating characteristic analysis for differentiation of FC from SCA and MCA. Details of area under the curves and 95% CIs of each index are shown in Results section.

Funding

This work was supported by a Grant-in-Aid for Scientific Research (C), Japan Society for the Promotion of Science (JSPS), Japan KAKENHI Grant Number 18K07683.

Declaration of Competing Interest

The authors have no conflicts of interest to declare.

Acknowledgments

The authors thank Professor Seiko Kato, MD, PhD, Department of Gynecology and Obstetrics, Graduate School of Medical Sciences, Kyushu University, and Professor Yoshinao Oda, MD, PhD, Department of Anatomic Pathology, Graduate School of Medical Sciences, Kyushu University, for providing the clinical information for this article and Jochen Keupp, PhD, Phillips Research, for his advice about APT imaging pulse sequences.

References

[1] K.A. Cronin, A.J. Lake, S. Scott, R.L. Sherman, A.M. Noone, N. Howlader, S.J. Henley, R.N. Anderson, A.U. Firth, J. Ma, B.A. Kohler, A. Jemal, Annual report to the nation on the status of Cancer, part I: national cancer statistics, Cancer 124 (13) (2018) 2785–2800.
[2] S.A. Farghaly, Current diagnosis and management of ovarian cysts, Clin. Exp. Obstet. Gynecol. 41 (6) (2014) 609–612.
[3] P.V. Foti, G. Attina, S. Spadola, R. Caltabiano, R. Farina, S. Palmucci, G. Zarbo, R. Zarbo, M. D'Arrigo, P. Milone, G.C. Ettorre, MR imaging of ovarian masses: classification and differential diagnosis, Insights Imaging 7 (1) (2016) 21–41.
[4] N. Lalwani, S.R. Prasad, R. Vikram, A.K. Shanbhogue, P.C. Huettner, N. Fasih, Histologic, molecular, and cytogenetic features of ovarian cancers: implications for diagnosis and treatment, Radiographics 31 (3) (2011) 625–646.
[5] L. Saba, S. Guerriero, R. Sulcis, B. Virgilio, G. Melis, G. Mallarini, Mature and immature ovarian teratomas: CT, US and MR imaging characteristics, Eur. J. Radiol. 72 (3) (2009) 454–463.
[6] C.M. Glastonbury, The shading sign, Radiology 224 (1) (2002) 199–201.
[7] K.M. Ward, A.H. Aletras, R.S. Balaban, A new class of contrast agents for MRI based on proton chemical exchange dependent saturation transfer (CEST), J. Magn. Reson. 143 (1) (2000) 79–87.
[8] P.C. van Zijl, N.N. Yadav, Chemical exchange saturation transfer (CEST): what is in a name and what isn't? Magn. Reson. Med. 65 (4) (2011) 927–948.
[9] J. Zhou, J.F. Payen, D.A. Wilson, R.J. Traystman, P.C. van Zijl, Using the amide

proton signals of intracellular proteins and peptides to detect pH effects in MRI, Nat. Med. 9 (8) (2003) 1085–1090.
[10] J. Zhou, J.O. Blakeley, J. Hua, M. Kim, J. Laterra, M.G. Pomper, P.C. van Zijl, Practical data acquisition method for human brain tumor amide proton transfer (APT) imaging, Magn. Reson. Med. 60 (4) (2008) 842–849.
[11] A.N. Dula, L.R. Arlinghaus, R.D. Dortch, B.E. Dewey, J.G. Whisenant, G.D. Ayers, T.E. Yankeelov, S.A. Smith, Amide proton transfer imaging of the breast at 3 T: establishing reproducibility and possible feasibility assessing chemotherapy response, Magn. Reson. Med. 70 (1) (2013) 216–224.
[12] A. Nishie, Y. Asayama, K. Ishigami, Y. Ushijima, Y. Takayama, D. Okamoto, N. Fujita, D. Tsurumaru, O. Togao, K. Sagiyama, T. Manabe, E. Oki, Y. Kubo, T. Hida, M. Hirahashi-Fujiwara, J. Keupp, H. Honda, Amide proton transfer imaging to predict tumor response to neoadjuvant chemotherapy in locally advanced rectal cancer, J. Gastroenterol. Hepatol. 34 (1) (2019) 140–146.
[13] A. Nishie, Y. Takayama, Y. Asayama, K. Ishigami, Y. Ushijima, D. Okamoto, N. Fujita, D. Tsurumaru, O. Togao, T. Manabe, E. Oki, Y. Kubo, T. Hida, M. Hirahashi-Fujiwara, J. Keupp, H. Honda, Amide proton transfer imaging can predict tumor grade in rectal cancer, Magn. Reson. Imaging 51 (2018) 96–103.
[14] K.J. Park, H.S. Kim, J.E. Park, W.H. Shim, S.J. Kim, S.A. Smith, Added value of amide proton transfer imaging to conventional and perfusion MR imaging for evaluating the treatment response of newly diagnosed glioblastoma, Eur. Radiol. 26 (12) (2016) 4390–4403.
[15] Y. Takayama, A. Nishie, M. Sugimoto, O. Togao, Y. Asayama, K. Ishigami, Y. Ushijima, D. Okamoto, N. Fujita, A. Yokomizo, J. Keupp, H. Honda, Amide proton transfer (APT) magnetic resonance imaging of prostate cancer: comparison with Gleason scores, MAGMA 29 (4) (2016) 671–679.
[16] Y. Takayama, A. Nishie, O. Togao, Y. Asayama, K. Ishigami, Y. Ushijima, D. Okamoto, N. Fujita, K. Sonoda, T. Hida, Y. Ohishi, J. Keupp, H. Honda, Amide proton transfer MR imaging of endometrioid endometrial adenocarcinoma: association with histologic grade, Radiology 286 (3) (2018) 909–917.
[17] O. Togao, T. Yoshiura, J. Keupp, A. Hiwatashi, K. Yamashita, K. Kikuchi, Y. Suzuki, S.O. Suzuki, T. Iwaki, N. Hata, M. Mizoguchi, K. Yoshimoto, K. Sagiyama, M. Takahashi, H. Honda, Amide proton transfer imaging of adult diffuse gliomas: correlation with histopathological grades, Neuro Oncol. 16 (3) (2014) 441–448.
[18] O. Togao, J. Keupp, A. Hiwatashi, K. Yamashita, K. Kikuchi, M. Yoneyama, H. Honda, Amide proton transfer imaging of brain tumors using a self-corrected 3D fast spin-echo dixon method: comparison with separate B0 correction, Magn. Reson. Med. 77 (6) (2017) 2272–2279.
[19] O. Togao, A. Hiwatashi, J. Keupp, K. Yamashita, K. Kikuchi, T. Yoshiura, M. Yoneyama, M.J. Kruiskamp, K. Sagiyama, M. Takahashi, H. Honda, Amide proton transfer imaging of diffuse gliomas: effect of saturation pulse length in parallel transmission-based technique, PLoS One 11 (5) (2016) e0155925.
[20] P.E. Shrout, J.L. Fleiss, Intraclass correlations: uses in assessing rater reliability, Psychol. Bull. 86 (2) (1979) 420–428.
[21] E. Vinogradov, A.D. Sherry, R.E. Lenkinski, CEST: from basic principles to applications, challenges and opportunities, J. Magn. Reson. 229 (2013) 155–172.
[22] K. Kikuchi, K. Ishimatsu, S. Zhang, I.E. Dimitrov, H. Honda, A.D. Sherry, M. Takahashi, Presaturation power adjusted pulsed CEST: a method to increase independence of target CEST signals, Contrast Media Mol. Imaging 2018 (2018) 3141789.
[23] A. Velazquez, A. Reyes, J. Chargoy, A. Rosado, Amino acid and protein concentrations of human follicular fluid, Fertil. Steril. 28 (1) (1977) 96–100.
[24] S. Zheng, I.M. van der Bom, Z. Zu, G. Lin, Y. Zhao, M.J. Gounis, Chemical exchange saturation transfer effect in blood, Magn. Reson. Med. 71 (3) (2014) 1082–1092.
[25] X. Song, R.D. Airan, D.R. Arifin, A. Bar-Shir, D.K. Kadayakkara, G. Liu, A.A. Gilad, P.C. van Zijl, M.T. McMahon, J.W. Bulte, Label-free in vivo molecular imaging of underglycosylated mucin-1 expression in tumour cells, Nat. Commun. 6 (2015) 6719.